J Mater Sci (2010) 45:4682–4688
DOI 10.1007/s10853-010-4469-5

ULTRAFINE GRAINED MATERIALS

Analyses of route Bc equal channel angular pressing and post-equal channel angular pressing behavior by the finite element method

Eun Yoo Yoon · Ji Hoon Yoo · Seung Chae Yoon · Yong Keun Kim · Seung Chul Baik · Hyoung Seop Kim

Received: 12 February 2010 / Accepted: 3 April 2010 / Published online: 17 April 2010

Abstract Equal channel angular pressing (ECAP) process provides an efficient procedure for achieving ultrafine grained microstructures with excellent mechanical properties in metallic materials. In this article, a simulation scheme for predicting the mechanical behavior during and after ECAP was proposed. The proposed scheme was applied for interstitial-free (IF) steels, which are widely used for the automobile body applications. Plastic deformation behavior during several passes of ECAP in route Bc, including such aspect as deformed geometry, corner gap, forming load and strain uniformity, was predicted. Tensile testing responses of the ECAP-processed IF steel, including strain hardening, onset of necking, and post-necking behavior, were analyzed using the finite element method and compared with the experimental results. The predicted tensile curves, ultimate tensile strength, and elongation varying with the number of ECAP passes were in good agreement with experimental results. The computational scheme developed was demonstrated to successfully predict not only the plastic deformation behavior during ECAP but also the mechanical properties of the ECAP-processed material.

E. Y. Yoon · J. H. Yoo · H. S. Kim (✉)
Department of Materials Science and Engineering, Pohang University of Science and Technology (POSTECH), Pohang 790-784, Korea
e-mail: hskim@postech.edu; hskim@postech.ac.kr

S. C. Yoon
Research & Development Team, Hyundai HYSCO, Chungnam 343-831, Korea

Y. K. Kim
Advanced Materials R&D Center, Korea Institute of Industrial Technology (KITECH), Techno-Park Songdo, Incheon 406-130, Korea

S. C. Baik
POSCO, Seoul 135-777, Korea

Introduction

Severe plastic deformation (SPD) by equal channel angular pressing (ECAP) is a well-established technique, which has been used in the recent years for fabricating fully dense bulk samples with ultrafine/nanoscale-grained microstructures [1–4]. The die set for the ECAP process consists of two channels of equal cross section intersecting at an angle "Φ" ("channel angle") and a corner angle "Ψ" as shown in Fig. 1. A well-lubricated workpiece is placed in the entry channel and extruded into the exit channel by a punch or ram. The ECAP process can impose large plastic strains on the workpiece through repeated processes ideally by shear deformation, without varying the cross-sectional area of the workpiece. Many experimental and simulation studies have been carried out on the ECAP and various modified ECAP processes because the ECAP facilitates the production of nanostructured bulk samples with improved physical and mechanical properties without any impurities or residual porosity being introduced in the material, unlike bulk nanostructured materials manufactured from powders, which need further pressureless sintering processes [5–10].

Most publications on metallic materials fabricated by ECAP deal with materials having the fcc structure, particularly Al- and Cu-based systems. Reports on ECAP of bcc materials, such as Fe and ferritic steel, are rather scarce. The deformation behavior of bcc materials during ECAP as well as the evolutions of the microstructures and mechanical properties is still not well understood [10–13]. Especially, to get better properties in steels, there is a rising interest in

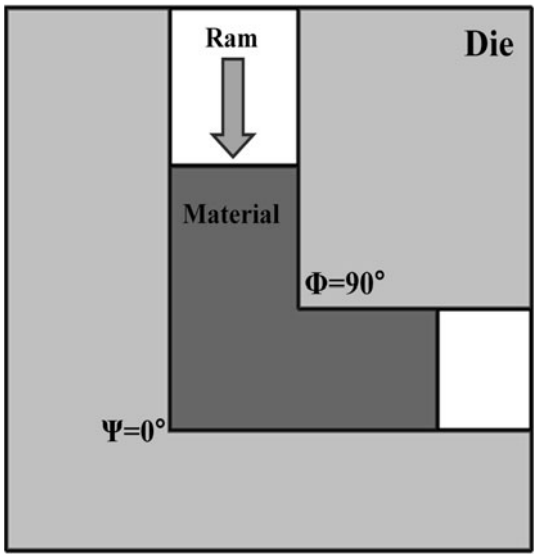

Fig. 1 Schematic of equal channel angular pressing

interstitial-free (IF) steels having a single phase ferritic microstructure and carbon steels. The micro-alloying elements (Ti, Nb, and V) in the IF steel form precipitates with carbon and nitrogen, rather than being dissolved interstitially in ferrite matrix. Deep drawing is a conventional sheet-forming process for automotive and electronic industries, where a sheet metal blank is deeply drawn into a die by the mechanical action of a punch. The absence of interstitial solutes and the appropriate texture in the IF steels lead to excellent deep drawability. Hence, the IF steel with very low carbon levels is widely used for automotive deep-drawing applications. Indeed, the IF steel is well suited for Galvanneal coating of automotive steel sheets and has excellent ductility, e.g., tensile elongation and formability, because of Mn, Si, and carbides in grain boundaries. On the other hand, low strength of the IF steels compared to advanced high strength steels, such as dual-phase (DP) steels, transformation-induced plasticity (TRIP) steels, twin-induced plasticity (TWIP) steels, etc., limits their industrial applications. An investigation of the ECAP-processed IF steel as a representative of single phase bcc materials would be not only of general scientific interest, but it may also demonstrate a practical applicability of SPD techniques for improving its mechanical properties thus opening up ways for broader applications of IF steels [13].

Owing to the industrial prospects of ECAP, intensive research in this area has been conducted, and significant progress has been made both in the understanding of fundamental properties (strength, fatigue, superplasticity, diffusivity, elasticity, internal friction, and corrosion) of the ECAP-processed materials and in analysis of the ECAP processing. For better understanding of the independent effects of various material and processing parameters and better process control, many studies on the effect of the various parameters on the ECAP process itself, and the properties of the ECAP products have been carried out by theoretical modeling. However, to the best of the authors' knowledge, simulation approaches that can predict the mechanical behavior *after* ECAP have not been tried yet.

In general, for assessing the reliability of the ECAP-processed materials, the mechanical properties are evaluated from their stress–strain curves. Kim et al. [14, 15] used Hart's necking instability condition [16] and addressed the effect of grain refinement on room temperature ductility of copper. In their results, it was demonstrated that room temperature ductility decreases with grain refinement in the submicrometer range. However, Hart's instability condition predicts the *onset* of necking and cannot give information on the post-necking behavior of tensile samples. It should be noted that failure of materials commonly occurs as rupture *after* the neck onset, rather than at the onset point itself. Hence, post-necking behavior, along with the necking onset instability, governs the ductility of the material. If growth of the neck is slow, then the material can maintain prolonged deformation from the onset of necking to the failure point. Therefore, it is of importance to investigate the tensile deformation and necking behavior using simulation approaches, e.g., the finite element method (FEM), especially for neck initiation and local neck growth in a post-necking stage [17, 18].

In this article, the post-necking behavior of ECAP-processed IF steels was investigated using a commercial FEM code. And ECAP processes of IF steel were also performed to provide a basis for comparison with the calculation results.

Experiments and finite element analysis

The material used in this investigation was an IF steel with a composition of 0.0026 wt% C, 0.0096 wt% Mn, 0.045 wt% Al, and 0.041 wt% Ti. The material was manufactured by the Pohang Steel Company (POSCO, Korea) and had the following history: After casting, the ingot was size-rolled to fabricate the plate 12 mm in thickness, homogenized for 1 h at 973 K, and then furnace-cooled. For ECAP processing, the billet was cut into 6 mm $\times$ 6 mm $\times$ 60 mm workpieces, which were annealed for 2 h at 973 K, furnace-cooled, and finally surface-polished using 1200 grit SiC paper. After the annealing treatment, the mean intercept grain size measured by optical microscopy was about 250 μm. The die parameters used in ECAP process, viz. the channel angle ($\Phi = 90°$) and the outer corner angle ($\Psi = 0°$) as shown in Fig. 1, yield a maximum von Mises effective strain of 1.155 for a single pass [19]. The ECAP process was conducted up to eight passes at

room temperature, following route Bc. Specifically, in route Bc, the workpiece was rotated through 90° around the longitudinal axis between the passes [5, 9]. The pressing speed was 1 mm/min, which is slow enough to maintain the temperature rise during ECAP within several degrees K. A mixture of MoS_2 powder and commercial oil was used for lubrication between the workpiece and the channel surfaces. For the characterization of mechanical behavior after ECAP, i.e., post-ECAP behavior, room temperature tensile tests were carried out using an MTS 810 machine with a constant cross-head speed of 0.001 mm/s, which corresponds to an initial strain rate of 1.4×10^{-4} s^{-1}.

An isothermal plane-strain FEM simulation of the ECAP process was carried out using the rigid-plastic commercial finite element code DEFORM2D V9.0 (http://www.deform.com). According to experimental [20] and theoretical [21–23] analyses, the constant temperature condition can be fulfilled at low pressing speeds. Therefore, the thermal effect due to heat of mechanical work was ignored. The shear friction factor between the inner surfaces of the die channel and the specimen was assumed to be 0.1, corresponding to a value commonly accepted in cold metal forming [24]. A constant ram speed of 1 mm/min was employed. The number of initial meshes of a four-node isoparametric plane-strain element was around 3000. This number of elements was found to be sufficient to represent local deformation of the strain rate insensitive workpieces through calculations with varying number of elements in DEFORM2D. The re-meshing function supported in DEFORM2D refines elements in strain concentration regions. A simplified constitutive relation for the material used in the simulations is Hollomon's equation derived from tensile tests, which returned the following values of the parameters involved: material strength factor $K = 499$ MPa and strain hardening exponent $n = 0.302$, see Fig. 2.

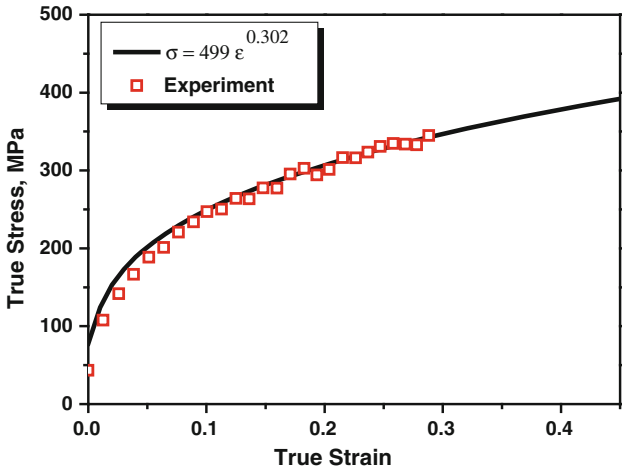

Fig. 2 The stress–strain curve of the material used in the simulation: Hollomon's equation with $K = 499$ MPa and $n = 0.302$ from tensile experiment results

Considering the computational efficiency and the experimental design of ECAP passes under route Bc rotating the ECAP samples through +90°, the two-dimensional (2D) simulational scheme [25] instead of the three-dimensional (3D) one, i.e., importing the variables of the previous ECAP pass to the simulation of the next one, was used. Figure 3 shows the 2D approximation scheme for the simulation of multiple pressings: the end state values (displacement, stress, and strain components) of a particular pressing were adopted as the initial values in the simulation of the subsequent pressing. State variables at the central element in a row of the workpiece were transferred to all the elements in the row for the next ECAP. This scheme had successfully been applied previously to routes B as well as A and C for deformation and texture predictions [25, 26].

Finite element method (FEM) was further applied to predict the flow curves as well as the tensile strength and elongation from the results of ECAP simulations. Figure 4 represents the method for selecting a calculation domain and the geometry for FEM simulation of tensile testing. The state variables of the ECAP-processed workpiece were first homogenized as the values in the central region, and used as initial values in the tensile testing simulations. It should be noted that the flow curve, effective stress versus

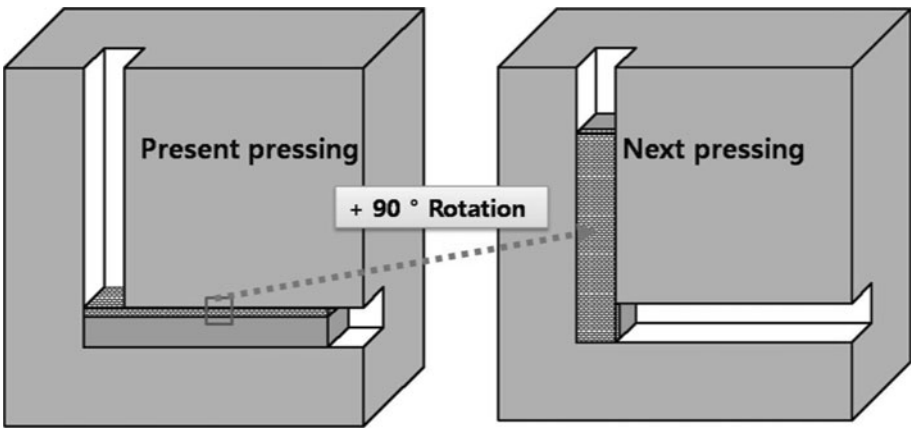

Fig. 3 2D schematic of equal channel angular pressing showing route Bc before the 2nd pressing

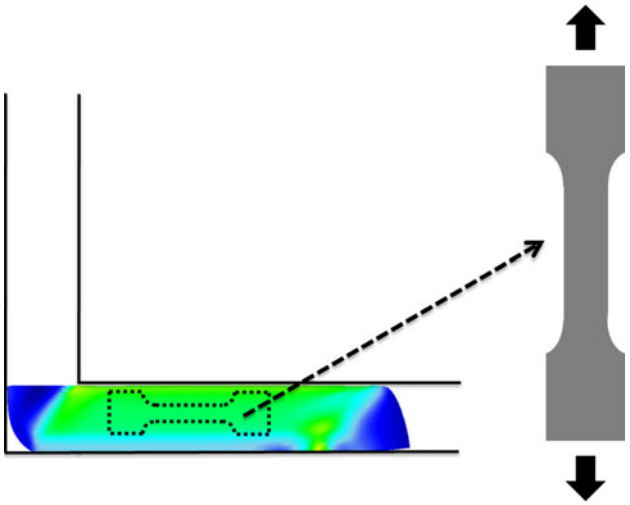

Fig. 4 Schematic of the simulation of the post-ECAP tensile testing

effective strain, was input into the FEM from the ECAP simulations. By means of analyzing and comparing the experiments and FEM simulations, theoretical analysis and predictions of necking onset and post-necking behavior of ECAP processed materials were evaluated.

Results and discussion

Figure 5 represents grain boundary images measured by electron backscatter diffraction (EBSD) of the initial IF sample, and ECAP-processed samples after the 1st, 2nd, 4th, and 8th passes. It was found that the grain size decreased with increasing number of passes, from initial 38.1 μm to 1.79, 1.21, 0.45, and 0.32 μm after the 1st, 2nd, 4th, and 8th pass, respectively. The initial sample had coarse grains (38.1 μm) with high angle boundaries. After the 1st and 2nd passes, many subgrains with the misorientation angle <15° were generated. After the 4th pass, stable high angle boundaries separating ultrafine grains, of size below 1 μm, tend to form. The average grain size in the eight-pass sample was about 150 nm. Mechanical properties of plastically deformed materials are affected by the strain path history. Accordingly, deformation histories were simulated using the FEM [4, 20–24].

Figure 6 shows the predicted effective strain distributions after several passes of route Bc ECAP. The average effective strain increases to about 0.83 after the 1st pass, about 1.93 after the 2nd pass, about 4.06 after the 4th pass, and about 8.25 after the 8th pass. The "steady state" region, i.e., the main part of the ECAP specimen excluding the head and tail parts, is where strain values do not vary along the pressing direction, and the strain profile does not vary along the width direction. The average strain evolution with the number of ECAP passes shows trends similar to those observed for the average effective strain experimentally (http://www.deform.com) [22] and in the 3D simulations [27]. Also, the strain distributions show inhomogeneous deformation features common to strain hardening materials [28]: (i) a large corner gap occurring in

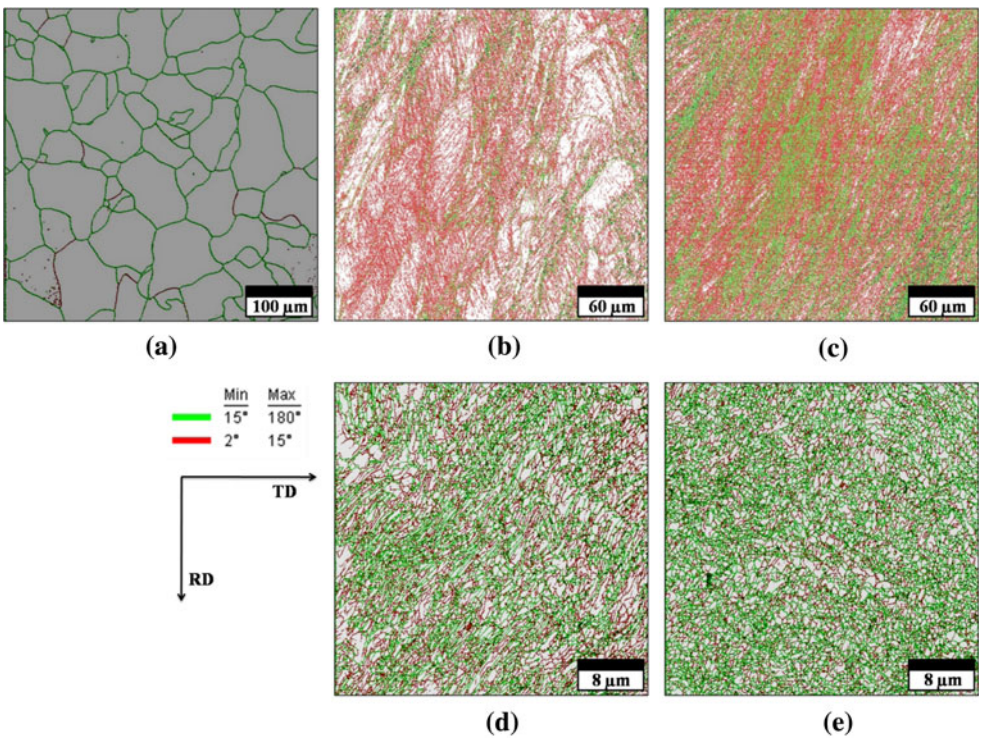

Fig. 5 Grain structure of IF steels for each ECAP pass measured by EBSD. **a** Initial, **b** 1 pass, **c** 2 passes, **d** 4 passes, **e** 8 passes

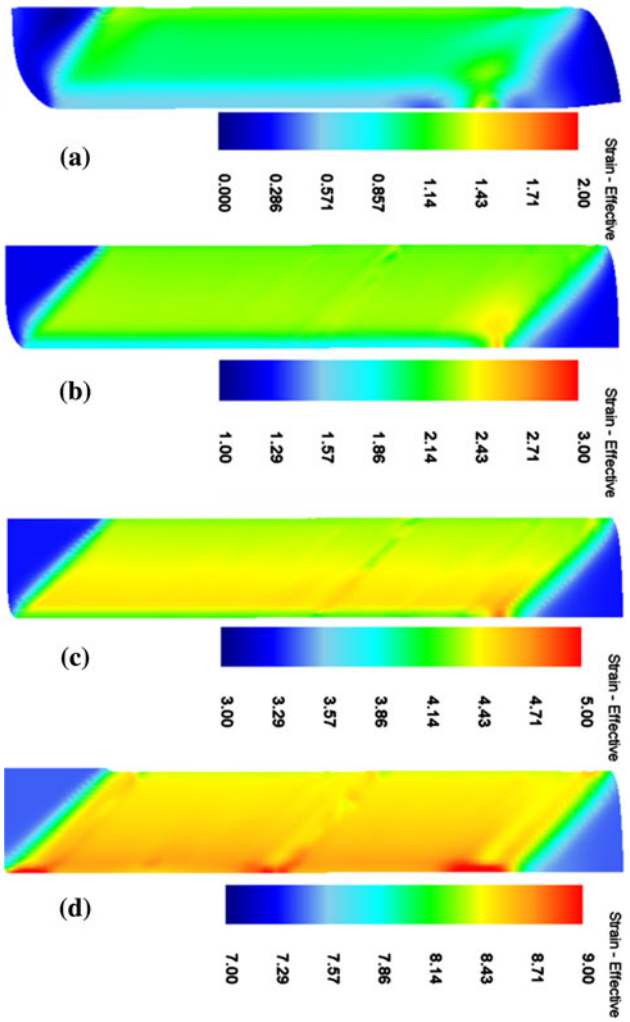

Fig. 6 Predicted effective strain distributions after equal channel angular spressing after **a** 1st, **b** 2nd, **c** 4th, and **d** 8th pass

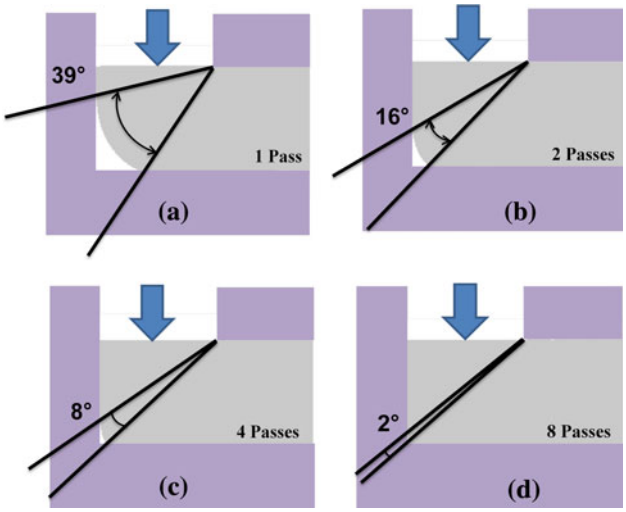

Fig. 7 FEM prediction of corner gap geometry changes along the path of the IF steel workpiece after ECAP processing after **a** 1st, **b** 2nd, **c** 4th, and **d** 8th pass

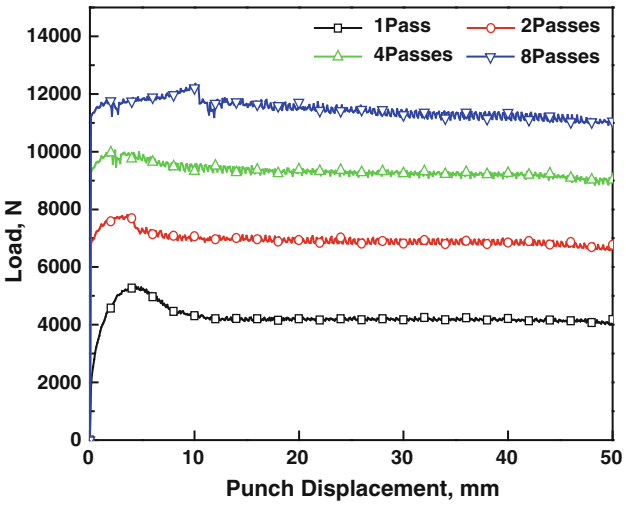

Fig. 8 Simulated pressing load versus displacement curves during ECAP processing of IF steels

strain hardening materials due to differences in stress and flow velocity between inside and outside regions, (ii) less sheared bottom zone due to a round corner angle or the corner gap, and (iii) front (leading edge of the sample), and rear (trailing edge of the sample) transient regions of the size comparable with the workpiece thickness. Evolution of the corner gap is shown in Fig. 7, the contour profiles at outer corner, to visualize the corner gap more clearly. It can be observed that the corner gap diminishes with the number of passes corresponding to an angle of 39°, 16°, 8°, and 2° after the 1st, 2nd, 4th, and 8th passes, respectively. As the number of passes increases, the strain hardening of the material decreases, hence, the corner gap angle also decreases. It is supported to raise the overall uniform deformation because of a decrease of a less deformed zone in the outer region with the number of ECAP passes. This result fits with the previous research very well [19, 28, 29]. The corner gap formation reduces the strain in the outside region of the workpiece, increases the strain in the inside region and decreases the average strain.

Figure 8 shows the calculated load versus ram displacement curves. It should be noted that three stages of the ECAP load can be distinguished in the first pass: initial load increasing, decreasing, and steady load stages. The difference in the load between passes decreases with increasing number of passes. The simulated peak load increases from 4,000 N after the 1st pass to 11,000 N after the 8th pass. This trend also reflects a continual decrease of the strain hardening rate with strain.

Tensile elongated geometries at the maximum load states in IF steel processed by various pass numbers of route Bc ECAP were drawn in Fig. 9a: 35% elongation

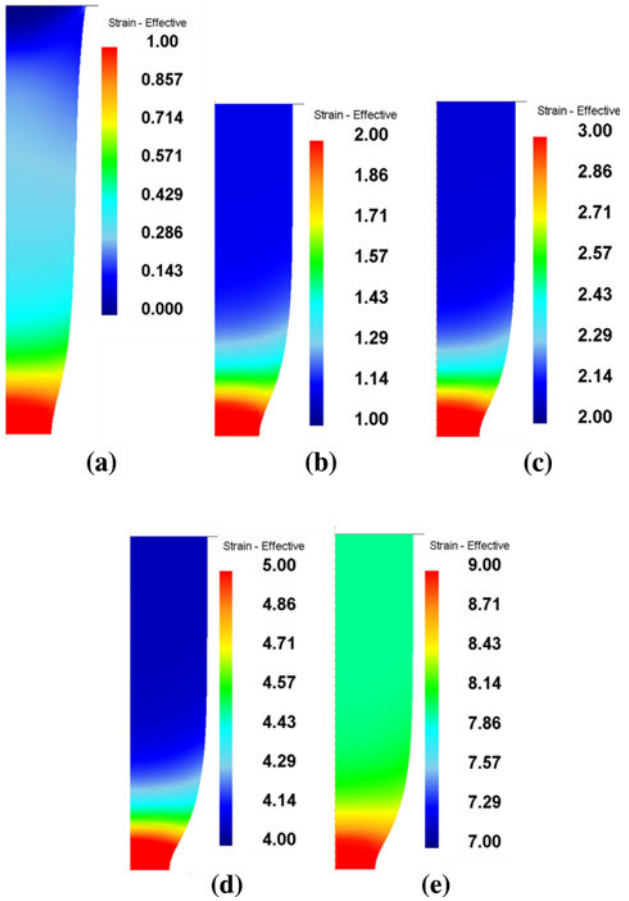

Fig. 9 FEM predictions of the elongated geometries with effective strain distributions in tensile samples after ECAP processing. **a** Initial IF steel, and after the **b** 1st, **c** 2nd, **d** 4th, and **e** 8th passes

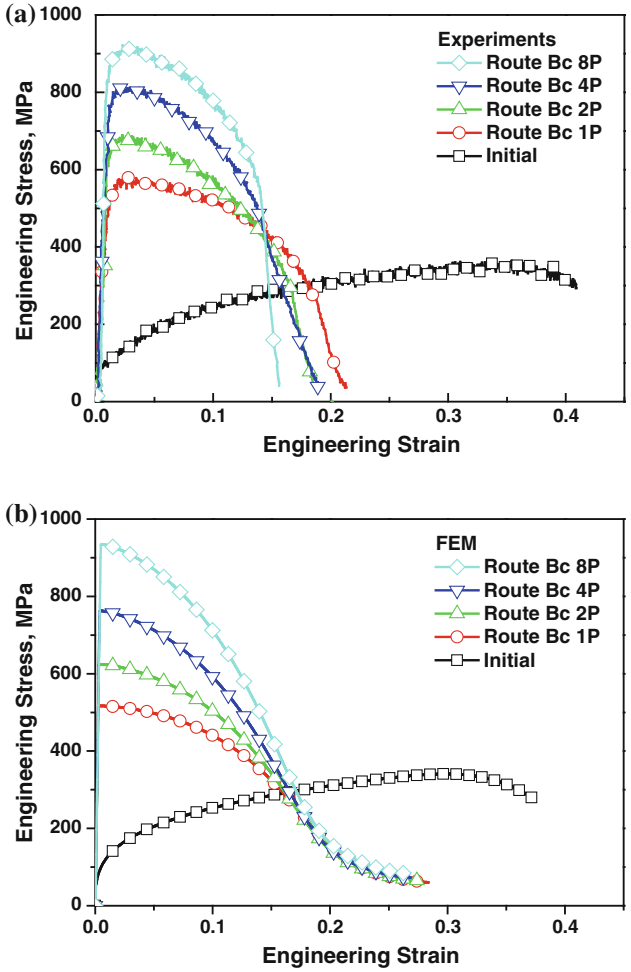

Fig. 10 Stress–strain curves after ECAP processing. **a** Experimental and **b** finite element method results

without ECAP processing, and Fig. 9b–e 4% elongation in the 1, 2, 4, and 8 passes in ECAP-processed samples. These states are the points where the tensile loads suddenly drop in the simulated tensile curves, see Fig. 10b. The sudden decrements in tensile loads coincide with the points where the minimum cross-sectional areas decrease precipitously due to the limits in load bearing capacity in the decreasing cross-sectional area. We identified these points as tensile elongation limits for IF steel in the corresponding ECAP-processed states. These tensile elongation limits are far from Hart's necking onsets, i.e., the beginning of tensile instability. As can be seen here, one of the benefits of the FEM is that post-necking behavior can be studied in detail. It should be noted that the strain values in the tensile samples are all different because of the different deformation histories. That is, strain vales below zero elongation in tensile tests are those accumulated during ECAP, the strain attained during tensile testing being added to the strain generated by ECAP.

Figure 10a, b shows experimental and simulated tensile flow curves, respectively, of initial and ECAP-processed samples. From Fig. 10a, it can be confirmed that materials can sustain a significant strain from the onset of necking to the failure point. In the case of initial sample in Fig. 10a, both the strain hardening stage and the uniform deformation stage are large. However, in the case of ECAP-processed samples, it can be observed that necking occurs at an early strain and the sample is fractured after around 15% elongation past the point of ultimate tensile strength (UTS). This amount of fracture strain in ECAP-processed IF steel is not sufficient for deep drawing: for example, strain in the square cup deep drawing benchmark test of Numisheet 1993 [30] reached 0.25. As the number of ECAP passes increases, the experimental UTS values are about 113, 695, 813, and 921 MPa in the initial sample, and after 2nd, 4th, and 8th pass ECAP, respectively. With growing number of ECAP passes, the UTS increases and a drop of stress after necking onset becomes more abrupt. The results of FEM simulations and the experimental results are in excellent agreement qualitatively and even

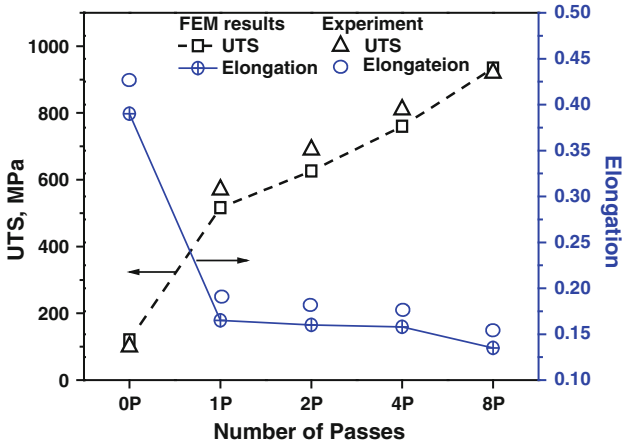

Fig. 11 Comparisons of the ultimate tensile stress and tensile elongation for IF steel as obtained by experimental and calculation methods

quantitatively. The variations of the UTS and the elongation are clearly confirmed by Fig. 11.

Conclusions

In this article, a simulation scheme, which utilizes importing of the values of the variable from a previous simulation step to the simulation of the subsequent one, was effectively used to predict the mechanical behavior during and after ECAP. The proposed scheme was applied for IF steels, which is used for the automobile body applications. The plastic deformation behavior of the IF steel during ECAP and the mechanical properties after ECAP processing were simulated. In uniaxial tensile tests of ECAP-processed IF steel, a high tensile strength of over 900 MPa and a tensile elongation of 15% were achieved by the eight passes of route Bc ECAP. Using a 2D approach for route Bc multistep ECAP processes, the observed behavior, with regard to a corner gap decrease and load increase, was adequately reproduced. Also, simulations of uniaxial tensile deformation of ECAP-processed IF steel using the FEM are in good accordance with the experimental results. Although for computational efficiency the simulations in this study were 2D, rather than 3D, both the behavior of the material under ECAP and the post-ECAP mechanical response were predicted very well. The simulation strategy used in this article shed some light on our understanding of the relation between the SPD processing and subsequent tensile behavior of IF steel.

For better understanding of the mechanical behavior, and particularly of the underlying microstructural mechanisms, physically based models [25, 26] need to be employed in place of an empirical constitutive equation used here. Such microstructure-related study is under way.

Acknowledgements This research was funded through a grant from the Center for Advanced Materials Processing (CAMP) of the 21st Century Frontier R&D Program funded by the Ministry of Science and Technology, Republic of Korea. This study was also supported by the second phase of the Brain Korea 21 Program in 2010. The calculations were performed availing the supercomputing resources of the Korea Institute of Science and Technology Information (KISTI).

References

1. Valiev RZ (2001) Metall Mater Int 7:413
2. Kim HS (1998) J Korean Inst Met Mater 36:2080
3. Valiev RZ, Islamgaliev RK, Alexandrov IV (2000) Prog Mater Sci 45:103
4. Kim HS, Hong SI, Seo MH (2001) J Mater Res 16:856
5. Valiev Z, Langdon TG (2006) Prog Mater Sci 51:881
6. Zhu YT, Liao XZ (2004) Nat Mater 3:351
7. Akhmadeev NA, Kobelev NP, Soifer RR, Ya M, Valiev RZ (1993) Acta Metall Mater 41:1041
8. Valiev RZ, Mulyukov RR, Ovchinnikov VV, Shabashov VA (1991) Scripta Metall Mater 25:841
9. Mulyukov KY, Khaphizov SB, Valiev RZ (1982) Phys Status Solidi 133:447
10. Moon BS, Kim HS, Hong SI (2002) Scripta Mater 46:131
11. Fukuda Y, Oh-ishi K, Horita Z, Langdon TG (2002) Acta Mater 50:1359
12. Hadzima B, Janeček M, Estrin Y, Kim HS (2007) Mater Sci Eng A 462:243
13. Kim HS, Ryu WS, Janeček M, Baik SC, Estrin Y (2005) Adv Eng Mater 7:43
14. Kim HS, Estrin Y (2001) Appl Phys Lett 79:4115
15. Kim HS, Estrin Y, Bush MB (2000) Acta Mater 48:493
16. Hart EW (1955) Acta Metall 3:146
17. Brünig M (1998) Finite Element Anal Des 28:303
18. Kim HS, Kim SH, Ryu WS (2005) Mater Trans 46:2159
19. Yoon SC, Hong SJ, Hong SI, Kim HS (2007) Mater Sci Eng A 449–451:966
20. Yamagichi D, Hoita Z, Nemoto M, Langdon TG (1999) Scripta Mater 41:791
21. Kim HS (2001) Mater Trans 42:536
22. Quang P, Krishnaiah A, Hong SI, Kim HS (2009) Mater Trans 50:40
23. Kim HS (2009) Mater Sci Eng A503:130
24. Altan T, Oh SI, Gegel HL (1983) Metal forming fundamental and applications. ASM, Metals Park, OH
25. Baik SC, Estrin Y, Hellmig RJ, Jeong HT, Brokmeier H-G, Kim HS (2003) Z Metallkd 94:1189
26. Baik SC, Estrin Y, Kim HS, Hellmig R (2003) Mater Sci Eng A 351:86
27. Mahallawy NE, Shehata FA, Hameed MAE, Aal MIAE, Kim HS (2010) Mater Sci Eng A527:1404
28. Kim HS, Seo MH, Hong SI (2000) Mater Sci Eng A 291:86
29. Şimşir C, Karpuz P, Gür CH (2010) Comput Mater Sci (submitted)
30. Makinouchi A, Nakamachi E, Onate E, Wagoner RH (1993) In: Proceedings of the Numisheet 1993 second international conference on numerical simulation of 3D sheet metal forming processes—verification of simulation with experiments, Isehara